

CHANDRA OBSERVATION OF V426 OPH: WEIGHING THE EVIDENCE FOR A MAGNETIC WHITE DWARF

LEE HOMER AND PAULA SZKODY

Astronomy Department, Box 351580, University of Washington, Seattle, WA 98195-1580

JOHN C. RAYMOND

Harvard-Smithsonian Center for Astrophysics, 60 Garden Street, Cambridge MA 02138

ROBERT E. FRIED¹

Braeside Observatory, P. O. Box 906, Flagstaff, AZ 86002

D.W. HOARD

SIRTF Science Center, California Institute of Technology, 1200 E. California Blvd, Pasadena, CA 91125

S. L. HAWLEY, M. A. WOLFE, J. N. TRAMPOSCH AND K. T. YIRAK

Astronomy Department, Box 351580, University of Washington, Seattle, WA 98195-1580

Accepted for publication in the Astrophysical Journal, April 3, 2019

ABSTRACT

We report the results of a 45 ks *Chandra* observation of the cataclysmic variable V426 Ophiuchus. The high resolution spectrum from the high-energy transmission grating spectrometer is most consistent with a cooling flow model, placing V426 Oph among the group of CVs including U Gem and EX Hya. An uninterrupted lightcurve was also constructed, in which we detect a significant 4.2 hr modulation together with its first harmonic at 2.1 hrs. Reanalysis of archival *Ginga* and *ROSAT* X-ray lightcurves also reveals modulations at periods consistent with 4.2 and/or 2.1 hrs. Furthermore, optical photometry in V, simultaneous with the *Chandra* observation, indicates a modulation anti-correlated with the X-ray, and later more extensive R band photometry finds a signal at ~ 2.1 hrs. The earlier reported X-ray periods at ~ 0.5 and 1 hrs appear to be only transient and quasi-periodic in nature. In contrast, the 4.2 hr period or its harmonic are stable and persistent in X-ray/optical data from 1988 to 2003. This periodicity is clearly distinct from the 6.85 hr orbit, and could be due to the spin of the white dwarf. If this is the case, V426 Oph would be the first long period intermediate polar with a ratio P_{spin}/P_{orb} of 0.6. However, this interpretation requires unreasonable values of magnetic field strength and mass accretion rate.

Subject headings: accretion, accretion disks — individual: V426 Ophiuchi — novae, cataclysmic variables — x-rays: stars

1. INTRODUCTION

The cataclysmic variable V426 Oph has proven to be somewhat enigmatic, even though it is a bright ($V=11.5-13.4$) system that has been studied for a number of years since its discovery as a nova-like with an emission line spectrum (Herbig 1960). A detailed spectroscopic study by Hessman (1988) revealed a K3 dwarf secondary in a 6.85 hr orbit with a white dwarf, with an inclination of 53° and at a distance of 200 pc. He concluded this was a Z Cam type of dwarf nova with outbursts approximately every 22 days and some standstills in the light curve occurring about one magnitude fainter than the outburst brightness. This interpretation would indicate V426 Oph is a system with such a high rate of mass transfer that it is very close to the upper limit for dwarf novae outbursts (Osaki 1996).

However, there are several observational clues that V426 Oph might also harbor a magnetic white dwarf. IUE observations show an unusually flat flux distribution in the UV, possibly indicating the truncation of a hot inner disk by a magnetic white dwarf (i.e. an intermediate polar), while the X-ray flux at quiescence is larger than for typical dwarf novae (Szkody 1986). The emission lines show flaring activity and a phase shift from a location near the white dwarf (Hessman 1988). Most importantly, quasi-periodic variability has been seen in the optical and X-ray at a period near 30 min at a brightness comparable to standstill (Szkody et al. 1990) and near 1, 2.5 or 4.5 hrs in the X-ray at quiescent brightness (Szkody 1986, Rosen et al. 1994; but see Hellier et al. 1990). While none of these periods could be positively identified as that of the rotation of the white dwarf to confirm the identification as an intermediate polar, the different brightness states combined with the lack of a long stretch of continuous observation have hampered attempts to resolve the origins of the observed periodicities.

With the advent of *Chandra*, high resolution X-

Electronic address: homer.szkody@astro.washington.edu

Electronic address: raymond@cfa.harvard.edu

Electronic address: hoard@ipac.caltech.edu

Electronic address: slh@astro.washington.edu

Electronic address: maw2323,jonica,ktirak@u.washington.edu

¹ Deceased

ray spectroscopy can be combined with uninterrupted long light curves to obtain much better information on the accreting regions of cataclysmic variables. Results are now available for the dwarf novae U Gem (Szkody et al. 2002), and WX Hyi (Perna et al. 2003), the intermediate polar EX Hya (Mauche et al. 2001), along with 5 other cataclysmic variables (Mukai et al. 2003). One of the surprising results is how similar the spectrum of the low mass accretion disk system U Gem is to that of the intermediate polar EX Hya. Mukai et al. (2003) have found that the seven systems can be divided into two groups. The first group, which includes U Gem and EX Hya, shows a bremsstrahlung continuum with strong H and He-like ion emission as well as ions from FeXVII-FeXXIV. The other group shows a harder X-ray continuum and little Fe L-shell emission. They suggest the differences in these two groups may be due to differences in the accretion rate per unit area. In the first group, the energy is released as optically thin radiation in a steady state cooling flow. In the second, the line emission arises from a plasma photoionized by the hard continuum. To further explore these ideas, and to try to resolve the nature of the accretion in V426 Oph, we obtained a *Chandra* observation at quiescence, together with simultaneous optical photometry and a single optical spectrum. We also obtained additional optical photometry (in quiescence) at a later date.

2. OBSERVATIONS

The *Chandra* observation of V426 Oph started at 21:40 UT on 2002 May 30 and ended at 11:02 UT the following day, with 45.15 ks of good exposure time on the source.

Differential photometry with respect to comparison star 1 in Misselt (1996) was accomplished with the Braeside Observatory (BO) 0.4m reflector using a SITe 512 CCD camera and a Bessell V filter on 2002 May 31 UT. Fifty second integrations for 4.4 hrs provided simultaneous overlap of 3.5 hrs with the *Chandra* data. Additional contemporaneous photometry was taken by the YALO 1m telescope at Cerro-Tololo Inter-American Observatory (CTIO). Using comparison stars 13, 14 and 15 (Henden & Honeycutt 1997), the V magnitude of V426 Oph was determined to be 12.79 ± 0.15 (YALO) and using star 1, between 12.7-12.9 (BO), consistent with a quiescent state. Observations on the AAVSO and VSNET web sites show that the previous outburst ($V \sim 11$) occurred on May 13-14.

On 2003 July 25 and 28 UT longer duration differential photometry in Harris R (4.0 hrs) and I (6.3 hrs) was obtained at Manastash Ridge Observatory (MRO), with its 0.75 m reflector. The exposure times were 30 and 10 s, respectively.

A single low resolution optical spectrum (6\AA) was also obtained during the *Chandra* observation, using the Double Imaging Spectrograph (DIS) on the 3.5m Apache Point Observatory (APO) telescope, providing spectral coverage from 3800-5200 \AA and 6000-8000 \AA (Figure 1). This spectrum also confirms that V426 Oph was at a quiescent state, exhibiting characteristic broad Balmer emission lines. All the observations are summarized in Table 1.

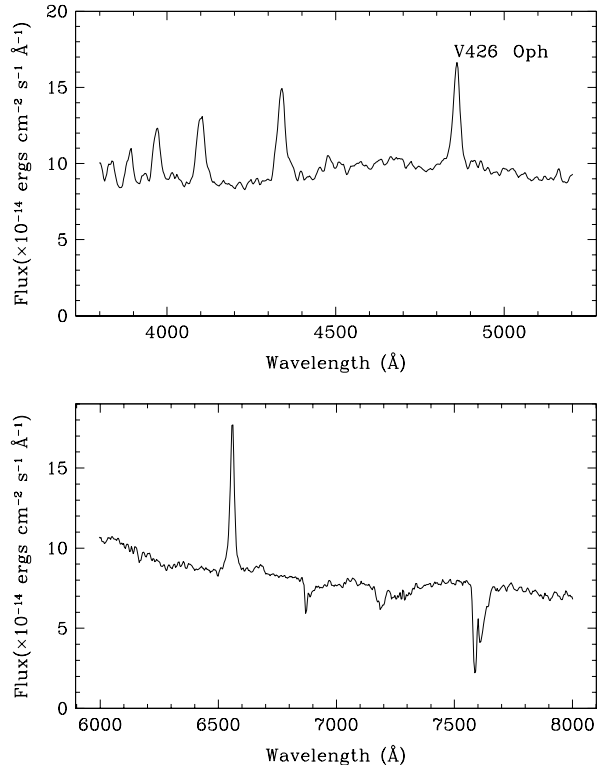


FIG. 1.— Low-resolution spectrum (6\AA) of V426 Oph obtained during the *Chandra* observation, note the broad Balmer emission lines.

3. X-RAY SPECTRAL ANALYSES AND RESULTS

We reprocessed our data starting from the level 1.5 event file, as advised by the *Chandra* X-ray Center. To check for intervals of high background we constructed an off-source lightcurve, but as none were found we were able to use the standard good time intervals as supplied. We chose to remove after-glow detection, as for these data it may have led to exclusion of good events. We applied destreaking to the S4 chip, to produce a clean level 2 event file, at the same time restricting our energy range to 0.3–10.0 keV, where calibrations are most reliable. We used `tgextract` to derive the type II pulse height analyzer (PHA) file. To achieve maximum signal-to-noise (S/N), we opted to add +1 and -1 grating orders, for both the medium (MEG) and high (HEG) energy grating spectra, creating type I PHA files. The script `add_grating_orders` also generated the appropriate grating response files for these co-added spectra. For high-resolution spectra it is generally advised to include the systematic sensitivity degradation of the ACIS chips (due to a build-up of absorbing material) as an independent model component. However we found that our S/N was insufficient to constrain the individual elemental abundances of the material. Instead, we corrected the ancillary response files (ARF) for the expected absorption at the time of observation, based on the nominal elemental composition. The HEG and MEG spectra are shown in Figure 2.

TABLE 1
OBSERVATION SUMMARY

UT Date	Obs	UT Time	Comments
2002 May 30, 31	Chandra: ACIS-S/HETGS	21:40 – 11:02	45.15 ks good time
2002 May 31	BO	07:04 – 11:30	V filter photometry
2002 May 30	CTIO: YALO	08:17 – 09:34	V filter photometry
2002 May 31	APO: DIS	06:20 – 06:25	spectrum
2003 July 25	MRO	06:00 – 10:04	R filter photometry
2003 July 28	MRO	04:35 – 10:51	I filter photometry

3.1. Cooling flow fits

First, in order to compare to earlier work we fitted a limited, mostly line free section of our spectrum from 2.0 to 5.0 keV with a simple thermal bremsstrahlung plus absorption model. Our best fit yielded a poorly constrained column of $N_H = 0.57 \pm 0.54 \times 10^{22} \text{cm}^{-2}$, and $kT_{Br} = 20 \pm 12 \text{keV}$, with a reduced $\chi^2_\nu = 0.51$ for 827 degrees of freedom. Both from this and simple inspection of the spectra we can see that V426 Oph belongs to the first group of CVs identified by Mukai et al. (2003); namely those best fit by a cooling flow as opposed to a photo-ionization model, with a maximum temperature nearer 20 than 80 keV.

We therefore proceeded to attempt a global cooling flow fit to our high-resolution spectra, using XSPEC² with the same model as Mukai et al. (2003). A suitable background file was obtained with the CIAO³ `tg_bkg` script. We used the FTOOL² `grppha` to associate the appropriate redistribution matrix (RMF), ARF and background files with the co-added first order grating PHA files. We also used `grppha` to group the spectra both simply binning by 4, then with binning to give ≥ 10 counts per bin. The S/N of our spectra is such that we opted to use the ≥ 10 counts per bin, and used χ^2 statistics for fitting.

In order to attain the best constraints possible we performed joint fits to both the HEG and MEG spectra, over wavelength ranges of 1.7–15 Å and 2.2–20 Å respectively, where counts are most adequate for fitting. Initially, we constrained the column to the $N_H = 0.7, 1.6$ and $0.28 \times 10^{22} \text{cm}^{-2}$ found by *EXOSAT*, *Ginga* and *ROSAT* observations respectively (Szkody 1986; Szkody et al. 1990; Rosen et al. 1994). The intermediate column from the *EXOSAT* spectrum gave the best fit, with $\chi^2_\nu = 0.55$. Indeed, with the column left free we achieved a best fit for $N_H = 1.0 \times 10^{22} \text{cm}^{-2}$, giving a $\chi^2_\nu = 0.47$ for 1718 d.o.f. The parameters for these four fits along with the corresponding 2–10 keV fluxes are summarized in Table 2, and the best model fit is over-plotted in Figure 2. As found for WX Hyi (Perna et al. 2003), we still find that our best fit model fails to fit any of the prominent lines at $\gtrsim 13 \text{Å}$ notably OVIII. Even setting low $T = 0.08 \text{keV}$, the minimum allowed in XSPEC, did not enhance these line fluxes noticeably.

Hence, we also experimented with several variations

² The X-ray software packages, XSPEC (spectral) and FTOOLS (general) are both available from <http://heasarc.gsfc.nasa.gov/docs/software/lheasoft/>

³ The Chandra data analysis software, CIAO, is available from <http://asc.harvard.edu/ciao/>

on the cooling flow model using a radiative shock wave code (Raymond 1979). We chose a shock speed of 4250km s^{-1} , to give a desired temperature of 22 keV, and complete electron-ion thermal equilibration. In this case, we compared the model results to specific line fluxes and ratios. IDL routines were used to extract background subtracted and binned data in wavelength and flux units for both HEG and MEG. To estimate line fluxes for the stronger lines we used the IRAF⁴ `splot` task to sum the flux over the width of the line above a continuum estimated by hand. For the weaker lines, important for line diagnostics (see next section), we instead used Gaussian fits to short segments of the MEG spectrum using binning with $S/N \geq 2$ per bin, constraining the line widths to be the same. The various line measurements are presented in Table 3.

The shock code allows us to examine the effects of photoionization. We can also make the flow nearly isobaric or nearly isochoric by adjusting the assumed magnetic field. These experiments showed that the line ratios are essentially independent of whether the flow is isobaric or isochoric, as expected, except that photoionization is relatively more important in the constant density case. Radiation from the cooling gas does affect the ionization state at the lower temperatures, but even for constant density cooling the effects are only 10–20% reductions in ratios such as O VIII/Fe XXV. A comparison of line intensities (Table 3) indicates that $N_H = 0.28 \times 10^{22} \text{cm}^{-2}$ best matches the O VIII intensity, while $N_H = 0.57 \times 10^{22} \text{cm}^{-2}$ does better for Ne X, Mg XII and Fe XVII. Within the restriction of the cooling flow model either value of N_H provides an adequate fit.

We also examined the effects of thermal conduction. As found by Perna et al. (2003) for the case of WX Hyi, thermal conduction transports energy to the cooler part of the flow, drastically increasing the strength of lines such as O VIII and Ne X. Even saturated thermal conduction (Cowie & McKee 1977) yields large ratios of low-T to high-T lines unless the conduction is strongly suppressed.

3.2. Line diagnostics

Mauche et al. (2001, 2004) have shown that the ratios of various Fe ion species can be a useful diagnostic for

⁴ IRAF (Image Reduction and Analysis Facility) is distributed by the National Optical Astronomy Observatory, which is operated by the Association of Universities for Research in Astronomy (AURA) Inc., under cooperative agreement with the National Science Foundation

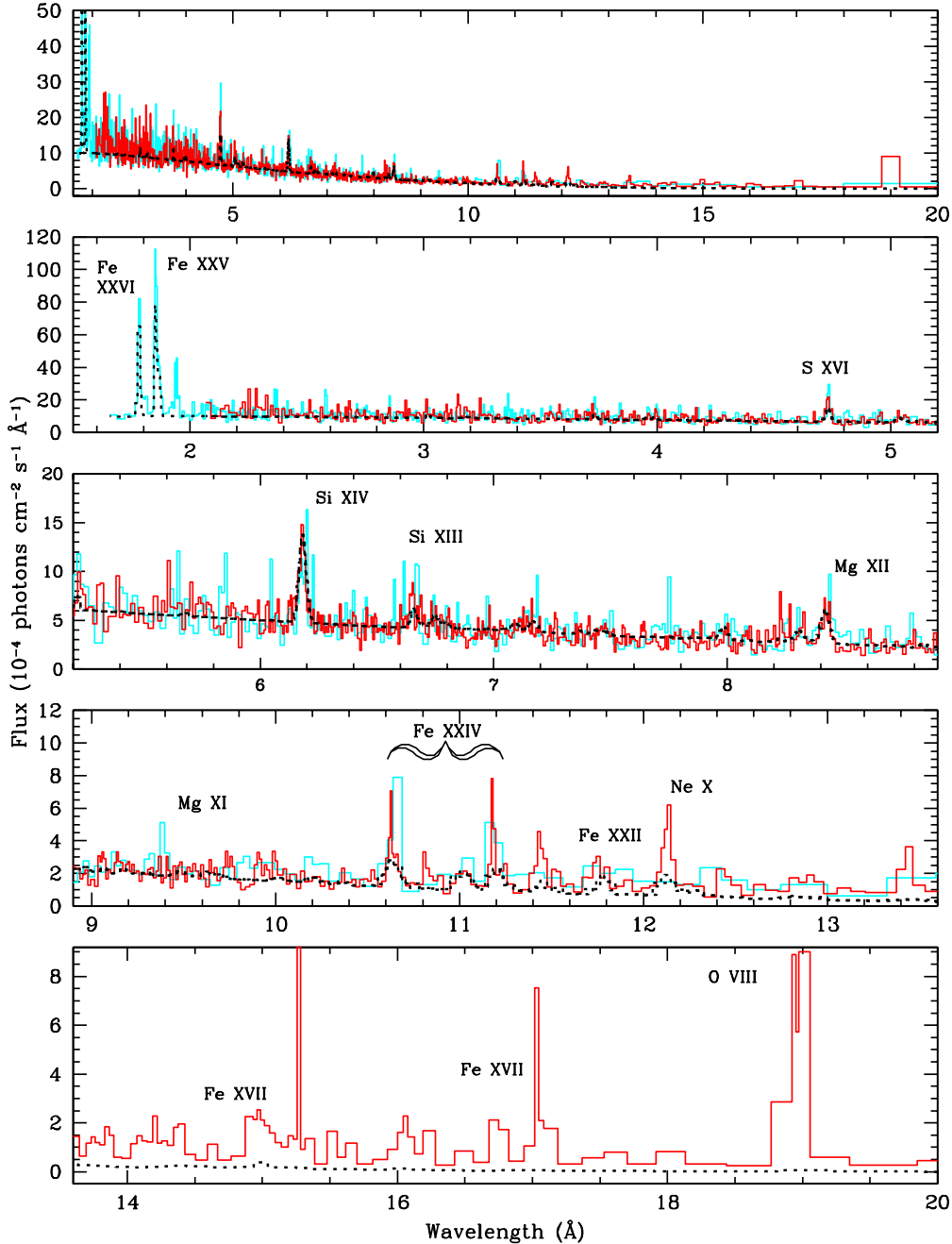


FIG. 2.— *Chandra*/HETGS unfolded spectrum of V426 Oph; both HEG (light grey, solid cyan in electronic edition) and MEG (dark grey, solid red in electronic edition) are shown. Overlaid is the best fit cooling flow model (dotted black). In the top panel we show an overview, while beneath we expand the wavelength scale and identify key emission lines. Note: the lowest panel shows the spectrum binned with $S/N \geq 2$ for clarity, the rest have ≥ 10 counts per bin.

the density of the line emitting plasma. Using our Gaussian line fits, we have calculated these ratios, which are presented alongside those of the Sun and EX Hya (from Mauche et al. 2001) in Table 4. Unfortunately, with our low S/N, the ratios for V426 Oph are only upper limits which are consistent with EX Hya, and only differ with the Sun in the ratios involving the 17.10 Å line. Thus, they do not provide useful diagnostics for the plasma

densities nor temperatures.

4. TEMPORAL ANALYSES AND RESULTS

4.1. *Chandra plus archival ROSAT and Ginga data*

The core of the *Chandra* 0th order image is significantly piled-up ($\sim 50\%$), hence this could not be used to construct a broad-band lightcurve. Instead, an event file was created from our reprocessed level 2 file, selecting only

TABLE 2
CRITICAL PARAMETERS FOR COOLING FLOW FITS

N_H (10^{22} cm^{-2})	low T (keV)	high T (keV)	Line width @ 6 keV σ_v (km s $^{-1}$)	\dot{M} ($M_\odot \text{ yr}^{-1}$)	χ^2_ν	2–10 keV flux ($10^{-11} \text{ erg cm}^{-2} \text{ s}^{-1}$)
0.28 ^a	0.9 ± 1.0	24.0 ± 0.9	600 ± 100	$9.6 \pm 0.8 \times 10^{-12}$	0.95	1.8 ± 0.2
0.7 ^a	1.1 ± 1.0	24.2 ± 0.9	500 ± 100	$1.3 \pm 0.2 \times 10^{-11}$	0.55	2.6 ± 0.4
1.6 ^a	1.1 ± 2.4	20.0 ± 1.1	600 ± 400	$1.9 \pm 0.5 \times 10^{-11}$	0.60	3.6 ± 0.9
1.0 ± 0.1	1.0 ± 0.2	24.2 ± 0.4	600 ± 100	$1.6 \pm 0.2 \times 10^{-11}$	0.47	3.0 ± 0.3

^aParameter values without uncertainties are fixed.

TABLE 3
LINE SUMMARY

Line	Rest λ Å	MEG Flux ^a	HEG Flux ^a	Shock	
				$N_H = 0.28 \times 10^{22} \text{ cm}^{-2}$	$N_H = 0.57 \times 10^{22} \text{ cm}^{-2}$
Fe XXVI	1.783	...	166	128	127
Fe XXV	1.850	...	191	216	214
S XVI	4.729	16	20	26.2	24.6
Si XIV	6.180, 6.187	13	11	30.2	26.6
Si XIII	6.647–6.688	6.8	9	17.7	15.2
Mg XII	8.419, 8.424	3.5	3.4	7.31	5.52
Fe XXIV	10.620–10.662	3.1	8.7	23.2 ^b	15.1 ^b
Fe XXIII	11.014	...	3.2	8.27	5.10
Fe XXIV	11.172, 11.189	2.2	4.4	27.0	14.8
Fe XXIV	11.429	2.3	1.5	10.0	5.33
Fe XXIII	11.740	1.6	...	13.7	6.86
Fe XXII	11.771	0.3	...	6.41	3.20
Ne X	12.128	3.1	...	12.4	6.18
Fe XVII	15.012	4.2	...	7.5	2.88
Fe XVII	16.774	2.8	...	3.35	0.73
Fe XVII	17.051	3.4	...	3.51	0.72
Fe XVII	17.098	<2.8	...	2.66	0.56
O VIII	18.970	5.9	...	17.7	3.29

^aflux units are $10^{-14} \text{ erg cm}^{-2} \text{ s}^{-1}$

^bModels are with the blend of Fe XXIV 10.620, 10.662

TABLE 4
FE XVII AND XXII LINE RATIOS

Ratio	Sun	EX Hya	V426 Oph
11.92/11.77	...	1.06	< 2
15.01/16.78	1.04	1.23	< 3.9
15.26/16.78	0.51	0.50	< 2.0
15.45/16.78	...	0.05	< 0.16
17.05/16.78	1.40	1.65	< 1.8
17.10/16.78	1.32	0.08	< 1.0
15.26/15.01	0.49	0.41	< 0.8
17.10/17.05	0.93	0.05	< 0.8

events in the 1.5 to 9.0 keV range, which corresponds to the peak of the source spectrum, hence minimizing background contributions. Extraction apertures were chosen to include only the wings of the 0th order image PSF, plus the brightest parts of the 1st order spectrum landing on the S3 and S4 chips; the areas close to chip boundaries were specifically excluded, since they have a reduced exposure fraction due to the spacecraft dither. As a cross-check, a lower signal-to-noise lightcurve using solely the PSF wings was subjected to the same analysis; fully-consistent results were found. The CIAO lightcurve

tool was used to extract a lightcurve with 200s bins, with background subtraction based upon corresponding regions each side of the dispersed spectra; this is plotted in Figure 3 (top panel).

To search for periodicities in the lightcurve, both a Lomb-Scargle (Scargle 1982) and Phase-Dispersion Minimization (Stellingwerf 1978) periodogram were calculated; the former is most sensitive to sinusoid modulations, while the latter is better for periodic signals with more irregular morphology. Significant peaks ($\gtrsim 99.99\%$ level) were found at two frequencies corresponding to 2.13 and 4.31 hours, as shown in Figure 3, lower left. We then directly fit the lightcurve with two sinusoids plus a second order polynomial to take into account any longer term trends. The 2.1 hr period is close enough to being the 1st harmonic of the 4.3 hr that we also constrained the periods to these values, leading to period determinations of 4.23 ± 0.05 and 2.12 ± 0.02 hrs. Indeed, these latter periods do produce a good fit to the data (see Fig. 3, top panel), with a reduced $\chi^2 = 3.03$ as compared to $\chi^2 = 3.01$ for the unconstrained. The total peak-to-peak amplitude is large at $65 \pm 5\%$. Interestingly these two periods are close to two of the candidate periods found by Rosen et al. (1994) in their *ROSAT* lightcurve. However, we note that we found no evidence for signals at either of

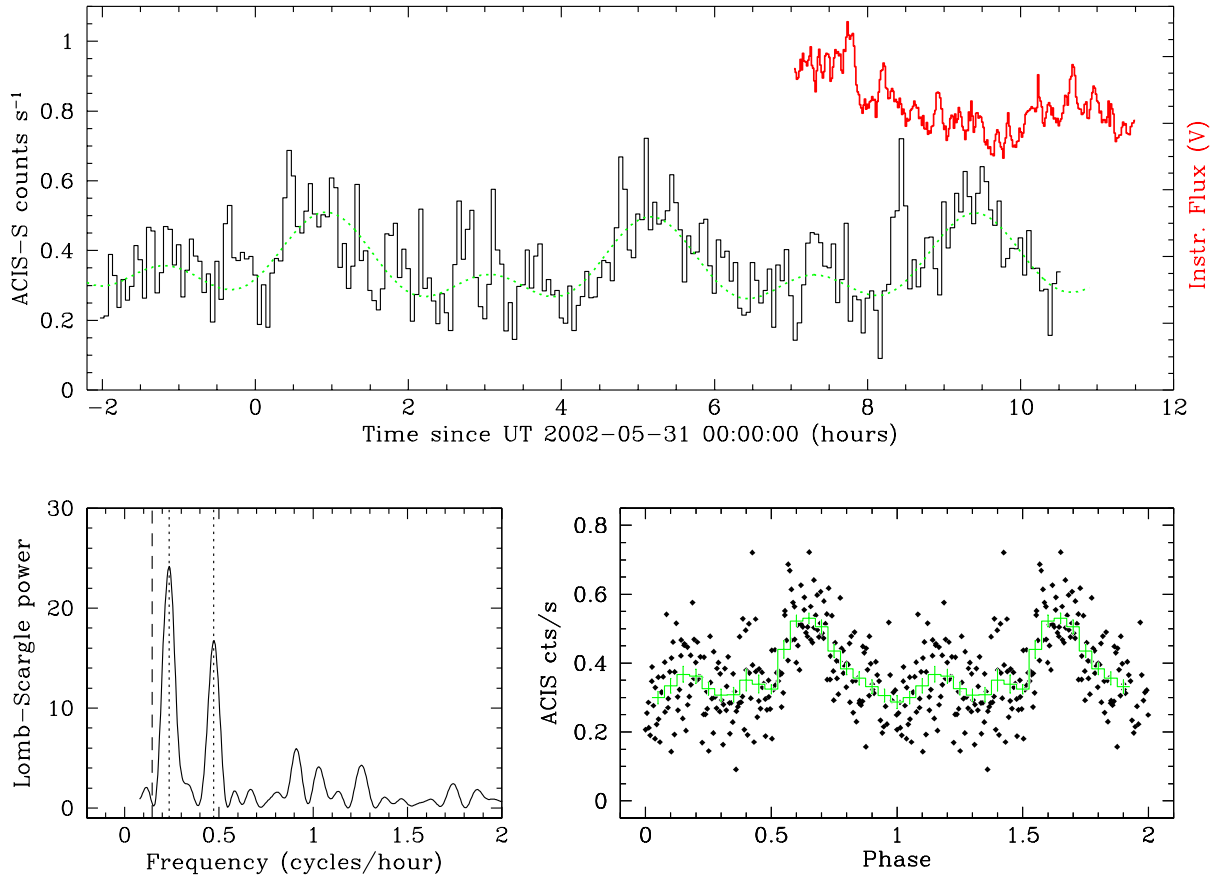


FIG. 3.— Top panel: Partly simultaneous lightcurves: lower, black curve— X-rays from *Chandra*/ACIS-S, and upper, dark grey (red in electronic edition) curve— optical (differential V band magnitudes converted to arbitrary count rate units for clarity). A double-sinusoid fit, with periods of 4.23 and 2.12 hrs, is over-plotted on the X-ray lightcurve. Lower left: Lomb-Scargle periodogram of the ACIS data. Two highly significant peaks ($> 99.99\%$ confidence) are apparent; the vertical bars indicate (left to right) the radial velocity determination of the binary orbital period (6.85 hrs), the fundamental of a double-sinusoid fit to the lightcurve (4.2 hrs) and its first harmonic (2.1 hrs). Lower right: The ACIS lightcurve folded on 4.2 hrs, and overlaid with binned values.

the putative short periods, ~ 60 min or ~ 30 min (Szkody 1986; Szkody et al. 1990), the binary orbit at 6.85 hrs (Hessman 1988) nor the 1.25 hr *ROSAT* candidate. Neither did we find signals at either of the spacecraft dither periods of 16.67 or 11.78 min, implying that we successfully excluded regions of reduced exposure fraction.

To compare directly to the *ROSAT* data, we extracted the archival 200s binned PSPC lightcurve from the HEASARC. The seven spectral bands were co-added to give us maximal S/N. We examined whether this data could also be fit by the periods we found in the high S/N uninterrupted *Chandra* lightcurve. A free fit found a period of 4.43 ± 0.08 hrs with $\chi^2_\nu = 3.24$, consistent with that found by Rosen et al. (1994), while if we constrained the period to 4.23 hrs the fit was not significantly worse with $\chi^2_\nu = 3.49$. We also attempted a double-sinusoid fit, as for the morphology seen in the *Chandra* data; here the modulation is in contrast best fit by a single sinusoid. Both single sinusoid fits are shown overlaid on the data in Figure 4.

The *Ginga* data have a long time-base (72 hrs) but, like *ROSAT*, interrupted sampling due to Earth oc-

tations. We obtained 64s binned lightcurves from the HEASARC, for the 2–6 keV range (where the spectrum peaks and S/N is best), then applied a quadratic detrend to remove longer term variations. The periodograms revealed evidence of significant flickering but peaks close to the 4.2 hr and its harmonic were by far the most significant. Once again a constrained double sinusoid fit yielded periods of 2.105 ± 0.005 hrs and 4.210 ± 0.010 hrs, consistent with the *Chandra* data. However, the fit has $\chi^2_\nu = 15$ for the 863 d.o.f, probably as a result of the extensive flickering, but also the morphology of the profile. In Fig. 5 we show folded and phase binned data, where the binning should average out the effects of flickering. Although the modulation is modulated primarily at the harmonic (2.1 hrs), the differing morphology of the two humps in the lower fold accounts for the significance of the 4.2 hr signal.

Hellier et al. (1990) reexamined the *EXOSAT* data in which Szkody (1986) detected a ~ 60 min periodicity and suggested an intermediate polar classification for V426 Oph. They concluded that the modulation was not in fact statistically significant. Moreover, they noted

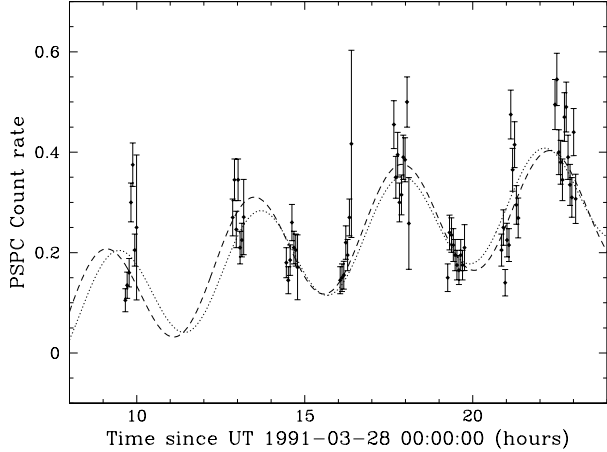


FIG. 4.— X-ray (0.5–2.5 keV) lightcurve from a *ROSAT*/PSPC pointed observation of V426 Oph. Overlaid are sinusoid fits, both a free fit (dashed line) with a period of 4.43 hrs, and another (dotted) with the period fixed at that found from the *Chandra* data, 4.23 hrs.

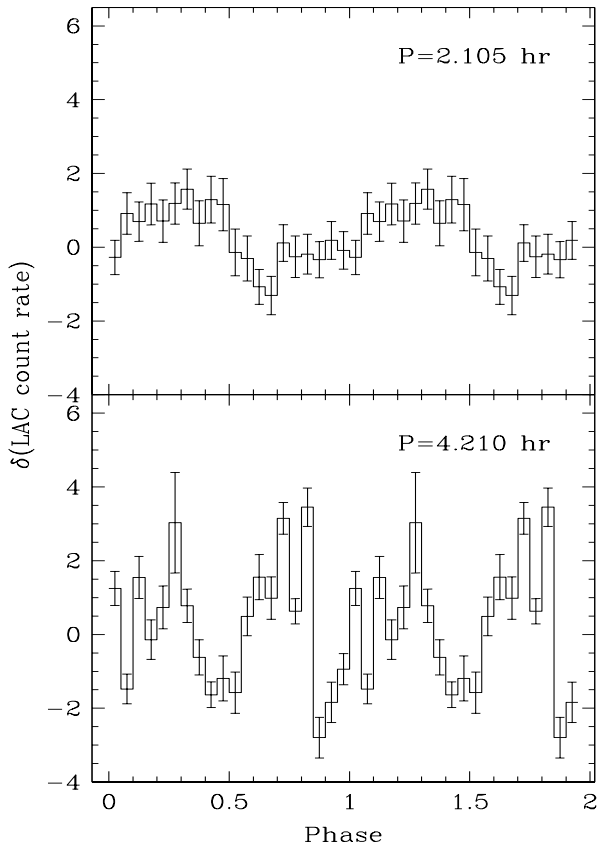


FIG. 5.— X-ray (2–6 keV) lightcurve from a *Ginga*/LAC pointed observation of V426 Oph. The data have been folded on periods of 2.105 hrs and 4.21 hrs respectively, then binned for clarity.

that the modulation on the white dwarf’s spin should be greatest at low energies, since it is due to absorption effects. Hence, the hardness ratio (hard/soft flux) should be anti-correlated with the total flux. We have investigated the energy dependence of our significant 4.23 hr

modulation. We extracted 800 s binned lightcurves in two energy bands, 0.3–2.5 keV for the soft and 2.5–6.0 keV for the hard, which approximately splits the counts evenly. In both bands the modulation is apparent, and indeed the signals are significant at $\gtrsim 99.95\%$ confidence level. Although the percentage amplitudes are different, with a hard band peak–peak amplitude of $59 \pm 5\%$ versus $73 \pm 6\%$ in the soft, the hardness ratio values are consistent with a constant, the signal at 4.23 hrs being merely 5% confidence. We also applied a Spearman rank correlation test comparing the hardness ratio with the full-band lightcurve. This yielded the expected anti-correlation though only at the 2σ level.

4.2. Optical results

We succeeded in obtaining optical photometry which overlaps the *Chandra* X-ray by 3.5 hours at the end of the observation. This lightcurve is plotted for ease of comparison in Figure 3 (top panel). Although the simultaneous coverage is limited, it is clear that the optical variability is in general *anti*-correlated with the X-ray, and that it also exhibits an ~ 4.2 hr periodicity. A Spearman rank correlation test yields an anti-correlation at the 3.7σ level.

Further quiescent lightcurves were obtained in 2003 July; the lightcurves, Lomb-Scargle periodograms and folded and phase binned data are presented in Figures 6 and 7. Once again fitting sinusoids, we find a modulation in the *R* data at a period consistent with the first harmonic of the 4.2 hr in the X-ray, 2.18 ± 0.06 hrs. The power spectrum also shows a number of significant peaks in the 20–50 min range, indicative of flickering. In the *I* band, the best fit period is 3.10 ± 0.03 hrs, similar to half that of the orbit, as expected for an ellipsoidal modulation. Indeed, adding a second sinusoid at double the period does improve the fit. However, in neither case are the periods formally consistent with those derived by Hessman (1988). On the other hand the lightcurve does not quite span a full orbit, and together with the irregular/quasi-periodic flickering, this may well account for the discrepancy. Lastly, removing the 3.1 hr sinusoid from the *I* data we find that a significant modulation ($> 99.0\%$ confidence) remains at 28.5 ± 0.1 min, which is in agreement with the X-ray (from *Ginga*) and optical periods presented by Szkody et al. (1990). Subdividing the lightcurve into four parts, we find that the amplitudes are comparable at both the minima and maxima of the 3.10 hr cycle, although the frequency does shift, indicating that this too is most likely only quasi-periodic flickering.

5. EVIDENCE FOR A MAGNETIC WHITE DWARF

5.1. Temporal

The classic signature of an IP is the presence of two or more coherent periodic modulations corresponding to the binary orbit, white dwarf spin and possibly their beat. In Table 5 we summarise all the periods reported for V426 Oph in the literature and from our own (re)analyses. The orbital period was definitively measured by Hessman (1988), whereas the existence of a second periodicity, the spin period, has been reported, revised and disputed over time (see Szkody 1986; Hellier et al. 1990; Szkody et al. 1990; Rosen et al.

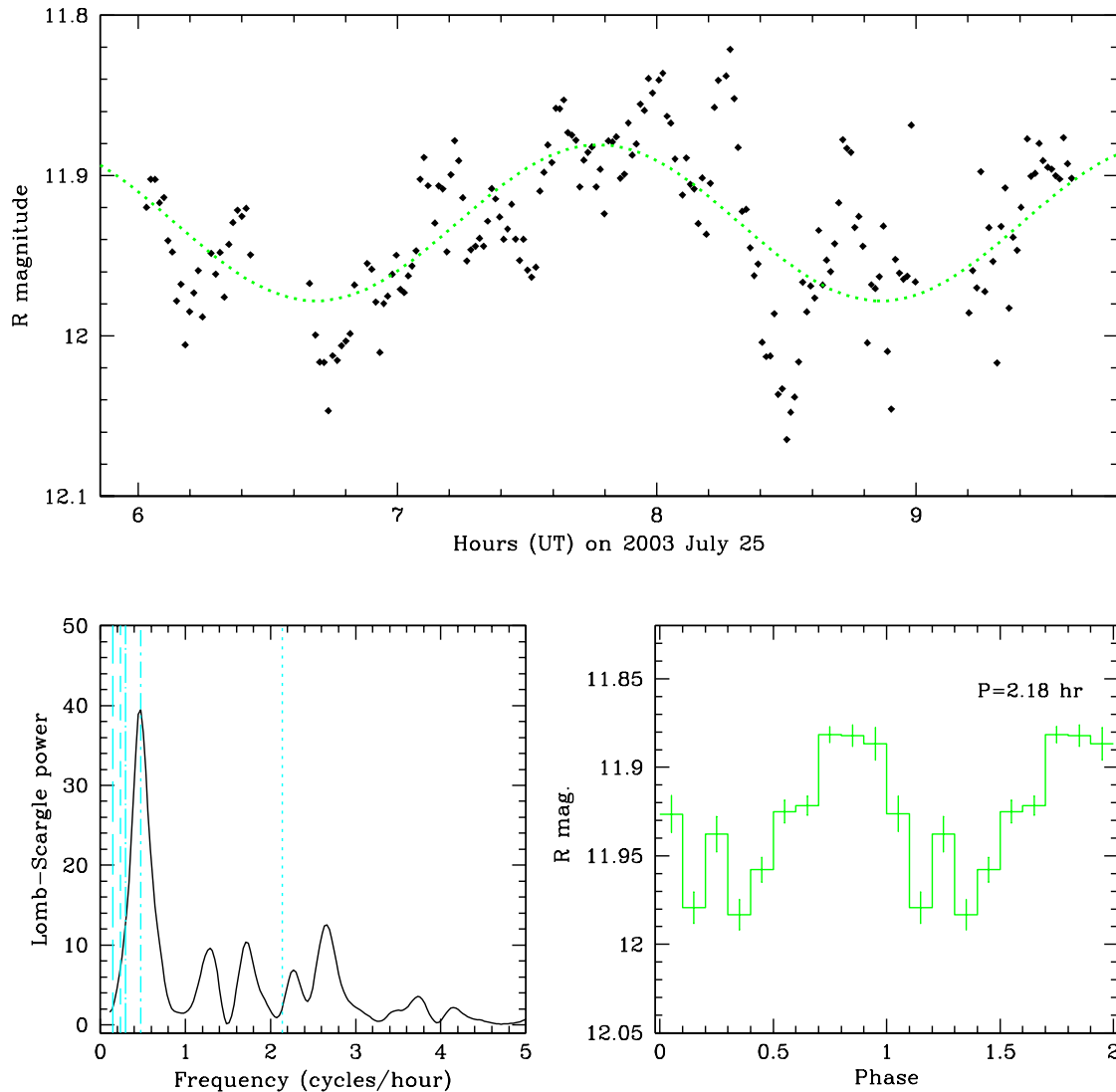


FIG. 6.— Top panel: Differential R band lightcurve of V426 Oph, a sinusoid fit with $P = 2.18$ hrs is over-plotted. Lower left: Lomb-Scargle periodogram of R data. A number of significant peaks ($> 99\%$ confidence) are apparent, the largest corresponding to the 2.18 hr modulation, while the rest are likely due to the prominent flickering. The vertical bars indicate (left to right) the radial velocity determination of the binary orbital period (6.85 hrs), the X-ray signal (4.2 hrs), first harmonic of the orbit (3.42 hrs), and the first harmonic of the X-ray signal (2.1 hrs), plus the 28 min period from *Ginga*. Clearly, the R band modulation is consistent with the first harmonic of the X-ray signal. Lower right: The R band lightcurve folded on 2.18 hrs and binned.

1994). The candidates (at ~ 0.5 and 1 hrs) are not, however, present in our long, uninterrupted *Chandra* dataset. We have found such periodicities in consecutive nights of optical photometry, but neither the modulation nor period are stable, the latter differing by $\sim 20\%$ from one night to the next. It seems most likely that these short periods are transient quasi-periodic behavior, possibly fairly stable flickering.

Instead, we have now found another, stronger candidate for the white dwarf spin period, at a surprisingly long period ~ 4.2 hrs. A similar periodicity (4.5 hrs) was first reported in the *ROSAT* observation, though this dataset has rather sparse sampling. In our *Chandra* lightcurve we have found a prominent modulation

at 4.23 hrs, with a probable first harmonic at 2.12 hrs, essentially consistent with the *ROSAT* result. Our re-analysis of the *Ginga* dataset has also uncovered the same period (to within the larger *Chandra* $\sim 1\%$ uncertainties), with the first harmonic dominating. Hence in X-rays either the 4.2 hr or its first harmonic appear persistently in observations from 1988 to 2002. Furthermore, the same periodicities are present in the optical (V and R bands), both in 2002 (simultaneous with the *Chandra* observations) and 2003. From the simultaneous observation we found a 180° phase offset between X-ray and optical modulations on the 4.23 hr period (note: a similar result was evident in the 28 min modulation observed in simultaneous *Ginga* and optical data, Szkody et al. 1990);

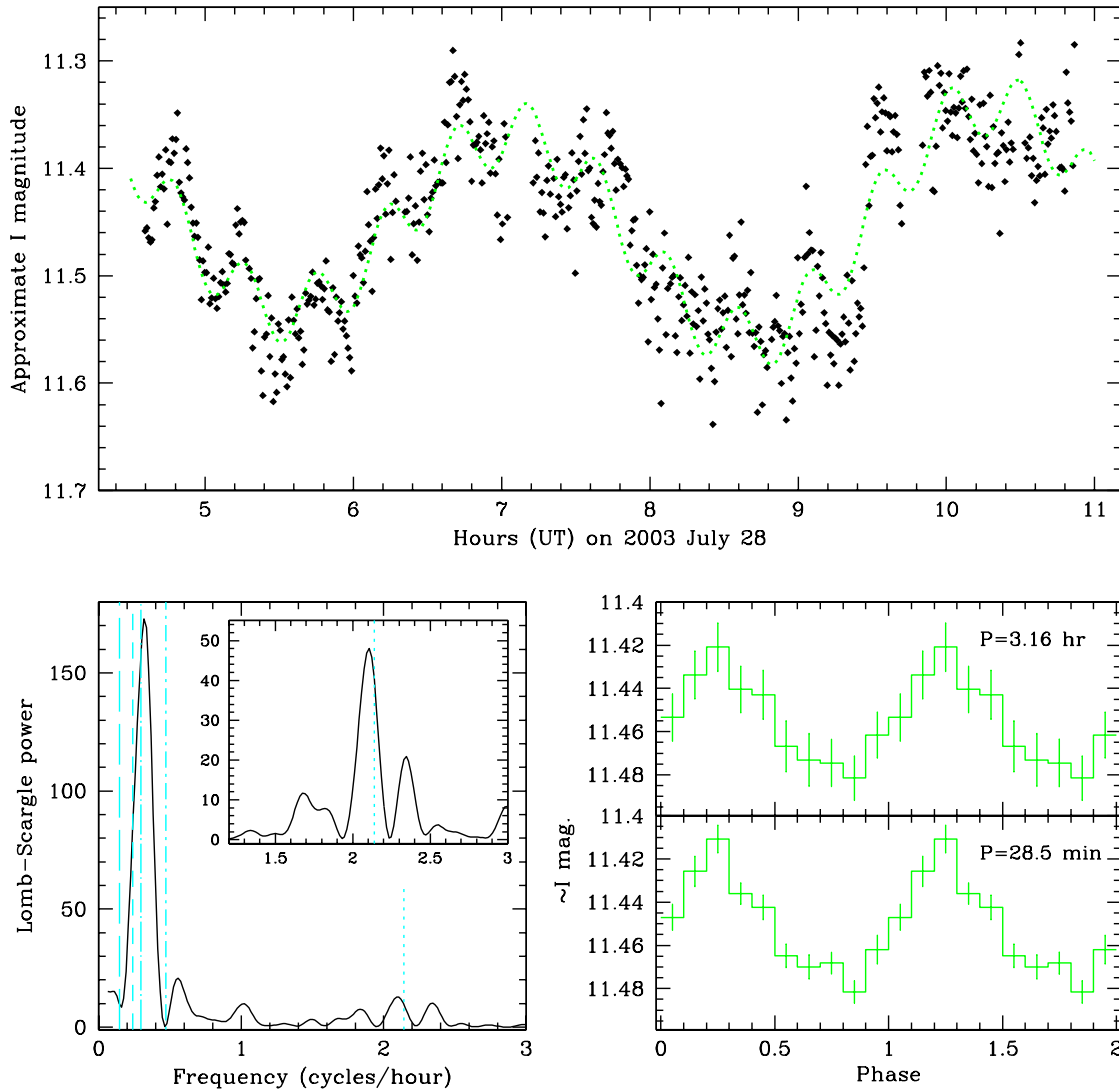


FIG. 7.— Top panel: Differential I band lightcurve of V426 Oph, a triple-sinusoid fit with $P = 3.16, 6.32$ hrs (modelling the expected ellipsoidal variation) and 28.5 min is over-plotted. Lower left: Lomb-Scargle periodogram of I data; the inset shows a close up in the vicinity of the 28.5 min peak, from data where the longer period sinusoids have been subtracted. A number of significant peaks ($> 99\%$ confidence) are apparent, the largest now corresponding to the 3.1 hr modulation, while the rest are likely due to the prominent flickering. The vertical bars indicate (left to right) the radial velocity determination of the binary orbital period (6.85 hrs), the X-ray signal (4.2 hrs), first harmonic of the orbit (3.42 hrs), and the first harmonic of the X-ray signal (2.1 hrs), plus the 28 min period from *Ginga*. The large peak is reasonably consistent with half the orbital period, whilst the signal at 28.5 min is close to that found by *Ginga*. However, we do note the presence of other peaks in that frequency range, indicating general flickering of which the 28.5 min signal happened to be the most significant. Lower right: The I band lightcurve folded on the periods shown and binned.

this is consistent with the effects of a reprocessed beam. Unfortunately, none of the X-ray data have sufficient S/N to test conclusively whether the modulation exhibits the expected energy dependence, but neither do they exclude that possibility. We should also note that the 4.2 hr signal is not apparent in a reanalysis of the 1988 optical spectroscopy (Hessman 2004, priv. comm.). However, in at least one other case, EX Hya during outburst (Hellier et al. 1989), it appears that any signal on the white dwarf spin, emitted from the magnetic disruption/corotation radius, is washed out by the line emission

from the outer disk.

While a white dwarf spin is the easiest explanation for the 4.2 hr period, the physical origin of this long P_{spin} is problematic. First, if we assume that V426 Oph possesses a fairly typical field for an IP (1–10 MG) and mass transfer rate of $10^{-9} - 10^{-10} M_{\odot} \text{yr}^{-1}$, then the Alfvén radius is $\sim 2 \times 10^{10}$ cm for spherical accretion, or half that in the disk case. Depending on the actual values used this radius could easily be smaller than both the radius of closest approach of the stream from the secondary and that of the initial ring that would form, hence formation

TABLE 5
SUMMARY OF DETECTED PERIODICITIES IN V426 OPH

Date	Observatory (keV)	State*	Wave band	Period (hrs)	Percentage amplitude	Identification	References
1980 June 15-17	Mt. Wilson	q	$H\beta$	6.0 ± 0.1	...	P_{orb}	2
1983 July 09-14	McDonald	q	Abs. lines	6.8475 ± 0.0023	...	P_{orb}	1
			$H\gamma, H\beta$	6.820 ± 0.076	...	P_{orb}	6
			Eq.W.	3.272 ± 0.009	...	$P_{orb}/2$ (?)	6
1984 Sept 25	EXOSAT/ME	q	X-ray(1.5–8.5)	1.00 ± 0.06	~30	Flickering (?)	2, 3
1988 Aug 8	SAAO ^a	q	$H\beta$ - V/R	~6.8	...	P_{orb}	3
			Eq.W.	~6.8, ~1.5	...	$P_{orb}/4$ (?)	3
1988 Sept 14–17	Ginga	ss	X-ray(2–6)	2.105 ± 0.005^b	26 ± 4	$P_{spin}/2$	4
				4.210 ± 0.010^b		P_{spin}	4
				0.47 ± 0.02	~10	Flickering (?)	5
1988 Sept 14–17	KPNO	ss	Optical: V	0.47(fixed)	~8	Flickering (?)	5
1989 July 06	SAAO	q	Optical: V	~2.2	~20	$P_{spin}/2$	3, 4
1991 Mar 28	ROSAT	...	X-ray (0.5–2.5)	4.43 ± 0.08	92 ± 8	P_{spin}	4
2002 May 30, 31	Chandra	q	X-ray(0.3–10)	4.23 ± 0.05^b	65 ± 5	P_{spin}	4
				2.12 ± 0.03^b		$P_{spin}/2$	4
2002 May 31	BO	q	Optical: V	~4.2	~20	P_{spin}	4
2003 Aug 25	MRO	q	Optical: R	2.18 ± 0.06	10 ± 1	$P_{spin}/2$	4
2003 Aug 28			Optical: I	3.16 ± 0.02^c	20 ± 1	$P_{orb}/2?$	4
				6.32 ± 0.04^c		$P_{orb}?$	4
				$0.475 \pm .002$	6 ± 1	Flickering (?)	4

REFERENCES. — (1) Hessman (1988). (2) Szkody (1986). (3) Hellier et al. (1990). (4) This paper. (5) Szkody et al. (1990). (6) Hessman (private communication)

* q – quiescence, ss – stand-still

^aSouth African Astronomical Observatory

^bPeriods constrained to ratio of 2, i.e. fundamental plus first harmonic

^cSinusoids constrained to be in-phase, with a period ratio of 2, in order to model the expected ellipsoidal modulation.

Note the formal uncertainty quoted here is almost certainly an underestimate.

of a disk is certainly possible (Warner 1995). However, if we also assume that the corotation radius is similar, one requires a $P_{spin} \sim 10$ min, while $P_{spin} = 4.23$ hrs would place the corotation radius outside the Roche lobe ($R_{co} \geq 9.0 \times 10^{10}$ cm as compared to the white dwarf- L_1 point separation $b \geq 7.8 \times 10^{10}$ cm). Even taking $P_{spin} = 2.1$ hrs, which is in itself difficult to reconcile with the data, leads to a corotation radius comparable to the size of a typical disk; hence the entire disk would be non-Keplerian and in a transitional state to full magnetic dominance. In addition, for disk-less accretion the size of the magnetic moment and in turn surface field are unreasonable, even taking $P_{spin} = 2.1$ hrs, we estimate $B_1 = 850(\dot{M} \times 10^{-9} M_{\odot} \text{yr}^{-1})$ MG.

An alternate model was put forward by King & Wynn (1999) to account for the spin-orbit equilibrium at $P_{spin}/P_{orb} = 0.68$ of the short period IP EX Hya. In this instance, the magnetic moment is such that the corotation radius is in fact comparable with the distance to the L_1 point. Norton et al. (2004) have more recently extended this work in an attempt to explain the entire range of spin-orbit equilibria seen for IPs. From their figure 2, we see that at $P_{orb} \equiv 7$ hrs, and $P_{spin}/P_{orb} = 0.6$, we are within the uncertainties of the model (which does assume $M_1 = 0.7 M_{\odot}$ in any case) in obtaining a suitable equilibrium. But a longer period (larger) system like V426 Oph requires $\mu \sim 10^{35} \text{Gcm}^{-3}$, or equivalently $B_1 \sim 300$ MG, comparable to the most magnetic polars.

An alternative non-magnetic origin for the 4.23 hr modulation could be stream overflow, which brightens a particular region of the disk. From Hessman (1988) tables III and IV, the Keplerian period at the

outer radius of the disk r_J is $P_{Kep}(r_J)/P_{orb} = (1 + q)^{1/2}(r_J/a)^{3/2} = 0.07$, which is much too small. Conversely, to obtain a ratio of 0.62, would require $q \sim 0.007$, again highly implausible.

A final possibility is that we could be seeing V426 Oph in an non-equilibrium state, where \dot{M} was greatly reduced on Myr timescales compared to what we now observe. However, this is an ad hoc assumption which has no satisfactory explanation.

5.2. Spectral

It is instructive to compare our spectral results on V426 Oph, with those of previous X-ray observations and Chandra results on other CVs. Given its Z Cam classification, the mass transfer rate for V426 Oph should be high. Instead the value $\sim 2 \times 10^{-11} M_{\odot} \text{yr}^{-1}$ places it in the middle of the five CVs that Mukai et al. (2003) fit with cooling flows. Moreover, we may compare this to an estimate of the mass accretion rate from the X-ray luminosity, $L_X(2-10 \text{keV}) = 8 \times 10^{33} \text{ergs}^{-1}$, which yields $\dot{M} = 7 \times 10^{-12} M_{\odot} \text{yr}^{-1}$, assuming half of the energy is released as X-rays. But as Perna et al. (2003) comment in the case of WX Hyi (where the cooling flow yields \dot{M} a factor of five less than obtained from fits to the UV continuum), these X-ray fits give \dot{M} in the outer disc, which may well not be accreting during quiescence, as the disk builds up for the next outburst.

As previously noted, for a thermal bremsstrahlung fit ($N_H = 0.7 \times 10^{22} \text{cm}^{-2}$, $kT_{Br} = 32$ keV), the EXOSAT data yielded a high 2–10 keV flux of $8 - 8.4 \times 10^{-11} \text{erg cm}^{-2} \text{s}^{-1}$, suggesting a magnetic system. For a thermal spectrum plus Fe line at 6.8 keV, the Ginga data

gave a flux value a factor of two lower, together with an even higher column ($1.6 \times 10^{22} \text{cm}^{-2}$), and a lower temperature ($kT_{Br} = 14 \text{ keV}$). However, at the time of the *Ginga* observation V426 Oph was in a stand-still state, close to outburst, hence the lower flux and higher column can be expected. Our *Chandra* observation provides another look at the quiescent state, but we have found a column and temperature intermediate between *EXOSAT* and *Ginga*, $1.0 \times 10^{22} \text{cm}^{-2}$ and $\sim 20 \text{ keV}$ respectively. Moreover, the flux given by the best cooling flow fit, $\sim 3 \times 10^{-11} \text{ erg cm}^{-2} \text{ s}^{-1}$ (2–10 keV), is much lower than either of the past satellite observations. Thus, it appears difficult to directly compare data taken at different outburst states and with different instrument sensitivities.

If V426 Oph contains a magnetic white dwarf, the X-rays should arise from a cooling region behind the accretion shock, and a shock model for the emission lines is appropriate. Mukai et al. (2003) found that polar spectra were better fit by models of photoionized plasma. Both polars and intermediate polars must have emission both from the cooling zone behind the accretion shock and from the photoionized gas upstream. The difference may be that polars have much narrower accretion columns and higher densities, and the recombination radiation from the photoionized accretion stream scales as the density squared. The emission per unit accreted mass from the shock, on the other hand, is independent of density. Ratios of lines from 3s and 3d levels of iron ions are a good diagnostic for photoionized plasmas (Liedahl et al. 1984), and the ratios of the Fe XVII lines and ratios of Fe XXIV lines confirm that the emission from V426 Oph originates in a collisionally ionized plasma.

The match between observed fluxes and the shock model is far from perfect, but it is close enough to indicate that the shock structure is basically correct. In particular, thermal conduction would tend to produce overly strong O VIII and Fe XVII lines unless it is suppressed by magnetic fields or turbulence. It is probably not advisable to make too much of the differences between the shock model and the observations at present, because accretion shocks are thermally unstable (Langer et al. 1982; Imamura et al. 1984). The instability and sec-

ondary shocks can modify the emission line spectrum at the factor of 2 level (Innes 1992).

6. CONCLUSIONS

Our analysis of a long uninterrupted *Chandra* X-ray lightcurve of V426 Oph together with optical photometry and reanalysis of archival X-ray data, has revealed a persistent period at 4.2 hrs, unrelated to the known orbit. In contrast, we find that previous candidate spin periods seen in past X-ray studies at ~ 0.5 and 1 hrs are most likely non-persistent QPOs. Our simultaneous X-ray/optical photometry shows that the modulations are anti-correlated and therefore the variations must arise from different parts of the system; possibly due to the reprocessing of beamed X-radiation. Indeed, the period of 4.2 hrs is easiest to interpret as the rotation of the white dwarf, implying that V426 Oph is, after all, an IP, and making it the first long period IP with a similar spin-orbit equilibrium to EX Hya, $P_{spin}/P_{orb} \sim 0.6$. However, this interpretation leads to problems with the magnetic field strengths and mass accretion rates that are typical for intermediate polars.

The high-resolution spectrum places V426 Oph as a member of the group of CVs, including U Gem and EX Hya, where the X-rays are emitted from a cooling flow. Indeed, more detailed modeling of the line fluxes for such a shock model lends further support to the magnetic CV interpretation.

With the death of Bob Fried on November 13th, 2003 the CV community has lost an active and dedicated observer. We gratefully acknowledge his years of collaboration.

We are grateful to the referee, Rick Hessman, for his helpful review. Support for this work was provided by NASA through *Chandra* award GO2-3033X. This research has made use of data obtained through the High Energy Astrophysics Science Archive Research Center Online Service, provided by the NASA/Goddard Space Flight Center.

REFERENCES

- Cowie, L. L. & McKee, C. F. 1977, *ApJ*, 211, 135
 Hellier, C., o. Mason, K., Smale, A. P., Corbet, R. H. D., O'Donoghue, D., Barrett, P. E., & Warner, B. 1989, *MNRAS*, 238, 1107
 Hellier, C., O'Donoghue, D., Buckley, D., & Norton, A. 1990, *MNRAS*, 242, 32P
 Henden, A. A. & Honeycutt, R. K. 1997, *PASP*, 109, 441
 Herbig, G. H. 1960, *ApJ*, 131, 632
 Hessman, F. V. 1988, *A&AS*, 72, 515
 Imamura, J., Wolff, M., & Durisen, R. 1984, *ApJ*, 276, 667
 Innes, D. 1992, *A&A*, 256, 660
 King, A. R. & Wynn, G. A. 1999, *MNRAS*, 310, 203
 Langer, S., Chanmugam, C., & Shaviv, G. 1982, *ApJ*, 258, 289
 Liedahl, D., Kahn, S., Osterheld, A., & Goldstein, W. 1984, *ApJ*, 350, L37
 Mauche, C. W., Liedahl, D. A., & Fournier, K. B. 2001, *ApJ*, 560, 992
 Mauche, C. W., Liedahl, D. A., & Fournier, K. B. 2004, in *Magnetic Cataclysmic Variables: Proceedings of IAU Colloquium 190*, ed. M. Cropper & S. Vriellmann, ASP Conf. Ser., in press
 Misselt, K. A. 1996, *PASP*, 108, 146
 Mukai, K., Kinkhabwala, A., Peterson, J. R., Kahn, S. M., & Paerels, F. 2003, *ApJ*, 586, L77
 Norton, A., Somerscales, R., & Wynn, G. 2004, in *Magnetic Cataclysmic Variables: Proceedings of IAU Colloquium 190*, ed. M. Cropper & S. Vriellmann, ASP Conf. Ser., in press
 Osaki, Y. 1996, *PASP*, 108, 39
 Perna, R., McDowell, J., Menou, K., Raymond, J., & Medvedev, M. V. 2003, *ApJ*
 Raymond, J. C. 1979, *ApJS*, 39, 1
 Rosen, S. R., Clayton, K. L., Osborne, J. P., & McGale, P. A. 1994, *MNRAS*, 269, 913
 Scargle, J. D. 1982, *ApJ*, 263, 835
 Stellingwerf, R. F. 1978, *ApJ*, 224, 953
 Szkody, P. 1986, *ApJ*, 301, L29
 Szkody, P., Kii, T., & Osaki, Y. 1990, *AJ*, 100, 546
 Szkody, P., Nishikida, K., Raymond, J. C., Seth, A., Hoard, D. W., Long, K. S., & Sion, E. M. 2002, *ApJ*, 574, 942
 Warner, B. 1995, *Cataclysmic Variable Stars* (Cambridge University Press), 57